

ENCODING CORTICAL SURFACE BY SPHERICAL HARMONICS

Moo K. Chung¹, Richard Hartley², Kim M. Dalton¹ and Richard J. Davidson¹

¹*University of Wisconsin, Madison* and ²*Australian National University*

Abstract: There is a lack of a unified statistical modeling framework for cerebral shape asymmetry analysis in the literature. Most previous approaches start with flipping the 3D magnetic resonance images (MRI). The anatomical correspondence across the hemispheres is then established by registering the original image to the flipped image. A difference of an anatomical index between these two images is used as a measure of cerebral asymmetry. We present a radically different asymmetry analysis that utilizes a novel weighted spherical harmonic representation of cortical surfaces. The weighted spherical harmonic representation is a surface smoothing technique given explicitly as a weighted linear combination of spherical harmonics. This new representation is used to parameterize cortical surfaces, establish the hemispheric correspondence, and normalize cortical surfaces in a unified mathematical framework. The methodology has been applied in characterizing the cortical asymmetry of a group of autistic subjects.

Key words and phrases: Spherical Harmonics, asymmetry analysis, cortical surface, diffusion, heat kernel.

1. Introduction

Previous neuroanatomical studies have shown left occipital and right frontal lobe asymmetry, and left planum temporal asymmetry in normal controls (Barrick et al. (2005) and Kennedy et al. (1999)). These studies mainly flip the whole brain 3D MRI to obtain the mirror reflected MRI with respect to the mid-sagittal cross-section. Then the anatomical correspondence across the hemispheres is established and a subsequent statistical analysis is performed at each voxel in the 3D MRI. Although this approach is sufficient for the voxel-based morphometry (Ashburner and Friston (2000)), where we only need an approximate alignment of corresponding brain substructures, it may fail to properly align highly convoluted sulcal and gyral foldings of gray matter. In order to address this shortcoming inherent in 3D whole brain volume asymmetry analysis, we need a new 2D cortical surface based framework.

The human cerebral cortex has the topology of a 2D highly convoluted grey matter shell with an average thickness of 3mm. The outer boundary of the shell

is called the *outer cortical surface* while the inner boundary is called the *inner cortical surface*. Cortical surfaces are segmented from magnetic resonance images (MRI) using a deformable surface algorithm and represented as a triangle mesh consisting of more than 40,000 vertices and 80,000 triangle elements (MacDonald et al. (2000), Chung et al. (2003)) (Figure 1). We assume cortical surfaces to be smooth 2D Riemannian manifolds topologically equivalent to a unit sphere (Davatzikos and Bryan (1995)). A sample outer surface can be downloaded from <http://www.stat.wisc.edu/~mchung/software/hk/hk.html>. The detailed explanation on reading data, visualization and simple manipulation in MATLAB are given in the web link. The triangle mesh format contains information about vertex indices, the Cartesian coordinates of the vertices and the connectivity that tells which three vertices form a triangle. For any type of cortical surface mesh, if V is the number of vertices, E is the number of edges, and F is the number of faces or triangles in the mesh, the Euler characteristic χ of the mesh should be constant, i.e. $\chi = V - E + F = 2$. Note that for each triangle, there are three edges. Since two adjacent triangles share the same edge, the total number of edges is $E = 3F/2$. Hence, the relationship between the number of vertices and the triangles is $F = 2V - 4$. In the sample surface, we have 40,962 vertices and 81,920 triangles.

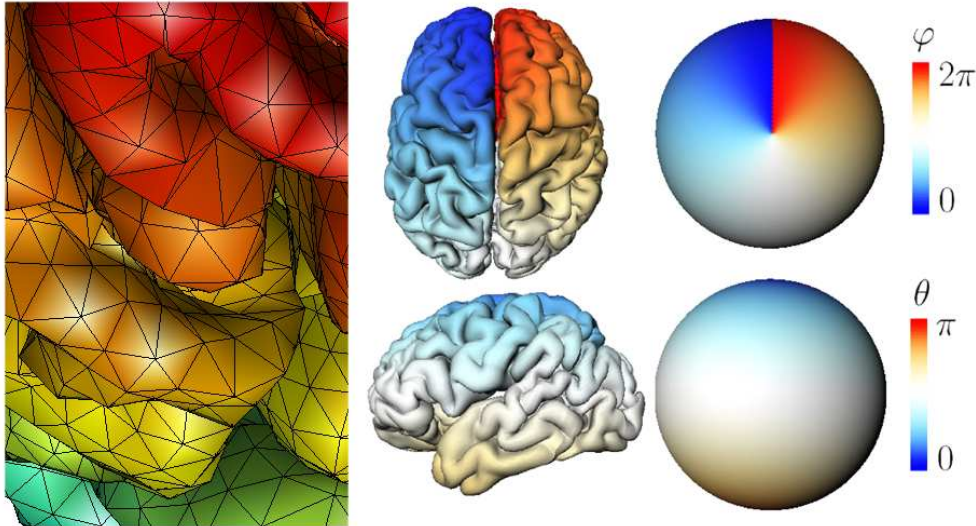


Figure 1. Left: The triangle mesh representation of the part of an outer cortical surface. The cortical thickness is measured at the vertices of the mesh. Right: Parameterization of cortical surface using the spherical coordinate system; the north and south poles are chosen in the plane, i.e. $u_2 = 0$, that separates the left and the right hemispheres.

Once we obtain the both outer and inner cortical surfaces of a subject, *cortical thickness*, which is the distance between the outer and inner surfaces, is computed at each vertices of the outer surface (MacDonald et al. (2000)). Since different clinical populations are expected to show different patterns of cortical thickness variations, cortical thickness has been used as a quantitative index for characterizing a clinical population (Chung et al. (2005)). Cortical thickness varies locally by region and is likely to be influenced by aging, development and disease (Barta, Miller and Qiu (2005)). By analyzing how cortical thickness differs locally in a clinical population with respect to a normal population, neuroscientists can locate the regions of abnormal anatomical differences in the clinical population. Cortical thickness serves as a metric of interest in performing 2D cortical asymmetry analysis. However, there are various methodological issues associated with using triangle mesh data. Our novel 2D surface modeling framework called the *weighted spherical harmonic representation* (Chung et al. (2007)) can address these issues in a unified mathematical framework.

Cortical surface mesh construction and cortical thickness computation are expected to introduce noise. To counteract this, surface-based data smoothing is necessary. For 3D whole brain volume-based method, Gaussian kernel smoothing, which weights neighboring observations according to their 3D Euclidean distance, has been used. However, for data that lie on a 2D surface, smoothing must be weighted according to the geodesic distance along the surface (Andrade et al. (2001), Chung et al. (2003)). It will be shown that the weighted spherical harmonic representation is a 2D surface-based smoothing technique, where the explicit basis function expansion is used to smooth out noisy cortical surface data. The basis function expansion corresponds to the solution of isotropic heat diffusion. Unlike the previous surface based smoothing that solves the heat equation nonparametrically (Andrade et al. (2001), Cachia et al. (2003), Chung et al. (2003), Chung et al. (2005)), the result of the weighted spherical harmonic representation is explicitly given as a weighted linear combination of spherical harmonics. This provides a more natural statistical modeling framework. A validation study showing the improved performance of the weighted spherical harmonic representation over heat kernel smoothing (Chung et al. (2005)) will be given in the paper.

Comparing measurements defined at mesh vertices across different cortical surfaces is not a trivial task due to the fact no two cortical surfaces are identically shaped. In comparing measurements across different 3D whole brain images, 3D volume-based image registration is needed. However, 3D image registration techniques tend to misalign sulcal and gyral folding patterns of the cortex. Hence, 2D surface-based registration is needed in order to compare measurements across different cortical surfaces. Various surface registration methods have been

proposed before (Thompson and Toga (1996), Davatzikos (1997), Miller et al. (1997), Fischl et al. (1999) and Chung et al. (2005)). These methods solve a complicated optimization problem of minimizing the measure of discrepancy between two surfaces. Unlike the previous computationally intensive methods, the weighted spherical harmonic representation provides a simple way of establishing surface correspondence between two surfaces in reducing the improper alignment of sulcal folding patterns without time consuming numerical optimization.

Once we establish surface correspondence between two surfaces, we also need to establish hemispheric correspondence within a subject for asymmetry analysis. However, it is not straightforward to establish a 2D surface-based hemispheric correspondence. Although there are many 3D volume-based brain hemisphere asymmetry analyses (Barrick et al. (2005), Kennedy et al. (1999)), due to this simple reason, there is a lack of 2D surface-based asymmetry analyses. This will be the first unified mathematical framework on 2D cortical asymmetry. The inherent angular symmetry presented in the weighted spherical harmonic representation can be used to establish the inter-hemispheric correspondence. It turns out that the usual asymmetry index of $(L-R)/(L+R)$ is expressed as the ratio between the sum of positive and negative order harmonics.

The novelty of our proposed method is that surface parameterization, surface-based smoothing, and within- and between- subject surface registration can be performed within a single unified mathematical framework that provides a more consistent modeling framework than previously available for cortical analysis.

2. Methods

Cortical thickness is measured at each vertex and used as a measure for characterizing cortical shape variation. There exists a bijective mapping between the cortical surface \mathcal{M} and a unit sphere S^2 that is obtained via the deformable surface algorithm. Consider the parameterization of the unit sphere S^2 given by

$$(u_1, u_2, u_3) = (\sin \theta \cos \varphi, \sin \theta \sin \varphi, \cos \theta),$$

with $(\theta, \varphi) \in [0, \pi) \otimes [0, 2\pi)$. The polar angle θ is the angle from the north pole and the azimuthal angle φ is the angle along the horizontal cross-section. Then, using the bijective mapping, we can parameterize the Cartesian coordinates $v = (v_1, v_2, v_3)$ of each cortical mesh vertex in the cortical surface \mathcal{M} with the spherical angles (θ, φ) , i.e., $v = v(\theta, \varphi)$ (Figure 1). This enables us to represent cortical thickness measurements f with respect to the spherical coordinates, i.e., $f = f(\theta, \varphi)$. Each component of surface coordinates will be modeled independently as

$$v_i(\theta, \varphi) = h_i(\theta, \varphi) + \epsilon_i(\theta, \varphi), \quad (2.1)$$

where h_i is the unknown smooth coordinate function and ϵ_i is a zero mean random field, possibly Gaussian. We model cortical thickness f similarly as

$$f(\theta, \varphi) = g(\theta, \varphi) + e(\theta, \varphi),$$

where g is the unknown mean cortical thickness and e is a zero mean random field. We further assume $v_i, f \in \mathcal{L}^2(S^2)$, the space of square integrable functions on unit sphere S^2 . The unknown signals h_i and g are then estimated in the finite subspace of $\mathcal{L}^2(S^2)$ spanned by harmonic basis functions in least squares fashion.

2.1. Spherical harmonics

The spherical harmonic Y_{lm} of degree l and order m is defined as

$$Y_{lm} = \begin{cases} c_{lm} P_l^{|m|}(\cos \theta) \sin(|m|\varphi), & -l \leq m \leq -1, \\ \frac{c_{lm}}{\sqrt{2}} P_l^{|m|}(\cos \theta), & m = 0, \\ c_{lm} P_l^{|m|}(\cos \theta) \cos(|m|\varphi), & 1 \leq m \leq l, \end{cases}$$

where $c_{lm} = \sqrt{[(2l+1)/2\pi][(l-|m|)!/(l+|m|)!]}$ and P_l^m is the *associated Legendre polynomial* of order m (Courant and Hilbert (1953) and Wahba (1990)). The associated Legendre polynomial is given by

$$P_l^m(x) = \frac{(1-x^2)^{\frac{m}{2}}}{2^l l!} \frac{d^{l+m}}{dx^{l+m}} (x^2-1)^l, x \in [-1, 1].$$

The first few terms of the spherical harmonics are

$$Y_{00} = \frac{1}{\sqrt{4\pi}}, Y_{1,-1} = \sqrt{\frac{3}{4\pi}} \sin \theta \sin \varphi, \\ Y_{1,0} = \sqrt{\frac{3}{4\pi}} \cos \theta, Y_{1,1} = \sqrt{\frac{3}{4\pi}} \sin \theta \cos \varphi.$$

The spherical harmonics are orthonormal with respect to the inner product

$$\langle f_1, f_2 \rangle = \int_{S^2} f_1(\Omega) f_2(\Omega) d\mu(\Omega),$$

where $\Omega = (\theta, \varphi)$ and the Lebesgue measure $d\mu(\Omega) = \sin \theta d\theta d\varphi$. The norm is then defined as

$$\|f_1\| = \langle f_1, f_1 \rangle^{\frac{1}{2}}. \quad (2.2)$$

Consider the subspace \mathcal{I}_l spanned by the l th degree spherical harmonics:

$$\mathcal{I}_l = \left\{ \sum_{m=-l}^l \beta_{lm} Y_{lm}(\Omega) : \beta_{lm} \in \mathbb{R} \right\}.$$

Then the subspace \mathcal{H}_k spanned by up to k th degree spherical harmonics is decomposed as the direct sum of $\mathcal{I}_0, \dots, \mathcal{I}_k$:

$$\begin{aligned}\mathcal{H}_k &= \mathcal{I}_0 \oplus \mathcal{I}_1 \cdots \oplus \mathcal{I}_k. \\ &= \left\{ \sum_{l=0}^k \sum_{m=-l}^l \beta_{lm} Y_{lm}(\Omega) : \beta_{lm} \in \mathbb{R} \right\}.\end{aligned}$$

Traditionally, the coordinate functions h_i are estimated by minimizing the integral of the squared residual within \mathcal{H}_k :

$$\hat{h}_i(\Omega) = \arg \min_{h \in \mathcal{H}_k} \int_{S^2} |v_i(\Omega) - h(\Omega)|^2 d\mu(\Omega). \quad (2.3)$$

It can be shown that the minimization is obtained when

$$\hat{h}_i(\Omega) = \sum_{l=0}^k \sum_{m=-l}^l \langle v_i, Y_{lm} \rangle Y_{lm}(\Omega). \quad (2.4)$$

Previously, representing an anatomical boundary via the Fourier series expansion (2.4) has been referred to as the *spherical harmonic representation* (Gerig et al. (2001), Gu et al. (2004), Shen et al. (2004) and Shen and Chung (2006)). This technique has been used in representing hippocampi (Shen et al. (2004)), ventricles (Gerig et al. (2001)) and cortical surfaces (Gu et al. (2004) and Chung et al. (2007)).

2.2. Weighted spherical harmonic representation

The weakness of the traditional spherical harmonic representation is that it produces the Gibbs phenomenon (ringing artifacts) (Gelb (1997) and Chung et al. (2007)) for discontinuous and rapidly changing continuous measurements. The Gibbs phenomenon can be effectively removed if the spherical harmonic representation converges fast enough as the degree goes to infinity. By weighting the spherical harmonic coefficients exponentially smaller, we can make the representation converges faster; this can be achieved by additionally weighting the squared residuals in equation (2.3) with the *heat kernel*. Figure 2 demonstrates the severe Gibbs phenomenon in the traditional spherical harmonic representation (top row) on a hat-shaped 2D surface. The hat-shaped step function is simulated as $z = 1$ for $x^2 + y^2 < 1$ and $z = 0$ for $1 \leq x^2 + y^2 \leq 2$. On the other hand the weighted spherical harmonic representation shows substantially reduced ringing artifacts. In both representations, we have used degree $k = 42$. For the weighted spherical harmonic representation, the bandwidth $\sigma = 0.001$ is used as it is through out the paper. Due to very complex folding patterns, sulcal

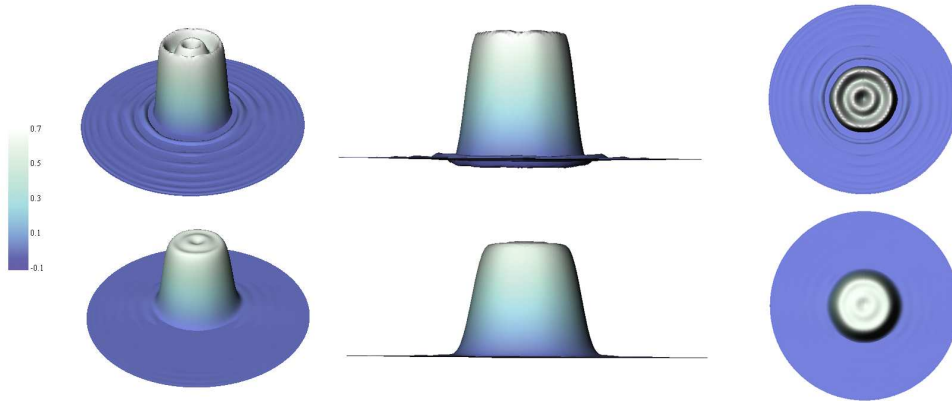


Figure 2. The Gibbs phenomenon on a hat shaped simulated surface showing the severe ringing effect on the traditional spherical harmonic representation (top) and reduced ringing effect on the weighted spherical harmonic representation (bottom). The degree $k = 42$ is used for the both cases and the bandwidth $\sigma = 0.001$ is used for the weighted spherical harmonic representation.

regions of the brain exhibit more abrupt directional change than the simulated hat surface (upward of 180 degree compared to 90 degree in the hat surface) so there is a need for reducing the Gibbs phenomenon in the traditional spherical harmonic representation.

The heat kernel is the generalization of the Gaussian kernel defined on Euclidean space to an arbitrary Riemannian manifold (Rosenberg (1997) and Chung et al. (2005)). On a unit sphere, the heat kernel is written as

$$K_{\sigma}(\Omega, \Omega') = \sum_{l=0}^{\infty} \sum_{m=-l}^l e^{-l(l+1)\sigma} Y_{lm}(\Omega) Y_{lm}(\Omega'), \quad (2.5)$$

where $\Omega = (\theta, \varphi)$ and $\Omega' = (\theta', \varphi')$. The heat kernel is symmetric and positive definite, and a probability distribution since

$$\int_{S^2} K_{\sigma}(\Omega, \Omega') d\mu(\Omega) = 1.$$

The parameter σ controls the dispersion of the kernel so we simply call it the *bandwidth*. The heat kernel satisfies $\lim_{\sigma \rightarrow \infty} K_{\sigma}(\Omega, \Omega') = 1/4\pi$ and $\lim_{\sigma \rightarrow 0} K_{\sigma}(\Omega, \Omega') = \delta(\Omega - \Omega')$ with δ as the Dirac-delta function. The heat kernel can be further simplified using the harmonic addition theorem (Wahba (1990)) as

$$K_{\sigma}(\Omega, \Omega') = \sum_{l=0}^{\infty} \frac{2l+1}{4\pi} e^{-l(l+1)\sigma} P_l^0(\Omega \cdot \Omega'), \quad (2.6)$$

where \cdot is the Cartesian inner product.

Let us define *heat kernel smoothing* (Chung et al. (2005)) as

$$K_\sigma * f(\Omega) = \int_{S^2} K(\Omega, \Omega') f(\Omega') d\mu(\Omega'). \quad (2.7)$$

Then heat kernel smoothing has the following spectral representation, which can be easily seen by substituting (2.5) into equation (2.7) and rearranging the integral with the summation:

$$K_\sigma * f(\Omega) = \sum_{l=0}^{\infty} \sum_{m=-l}^l e^{-l(l+1)\sigma} \langle f, Y_{lm} \rangle Y_{lm}(\Omega), \quad (2.8)$$

The k th degree finite series approximation of heat kernel smoothing is referred to as the *k th degree weighted spherical harmonic representation*. The unknown mean coordinates h_i are estimated using the weighted spherical harmonic representation, which is the minimizer of the of the weighted squared distance between measurements v_i and a function h in \mathcal{H}_k space. The unknown mean cortical thickness g is estimated similarly.

Theorem 1.

$$\begin{aligned} & \sum_{l=0}^k \sum_{m=-l}^l e^{-l(l+1)\sigma} \langle v_i, Y_{lm} \rangle Y_{lm} \\ &= \arg \min_{h \in \mathcal{H}_k} \int_{S^2} \int_{S^2} K_\sigma(\Omega, \Omega') |v_i(\Omega') - h(\Omega)|^2 d\mu(\Omega') d\mu(\Omega). \end{aligned}$$

Proof. Let $v_i = \sum_{l=0}^k \sum_{m=-l}^l \beta_{lm} Y_{lm}$. Let the inner integral be

$$I = \int_{\mathcal{M}} K_\sigma(\Omega, \Omega') \left| v_i(\Omega') - \sum_{l=0}^k \sum_{m=-l}^l \beta_{lm} Y_{lm}(\Omega) \right|^2 d\mu(\Omega').$$

Simplifying the expression, we obtain

$$\begin{aligned} I &= \sum_{l=0}^k \sum_{m=-l}^l \sum_{l'=0}^k \sum_{m'=-l'}^{l'} Y_{lm}(\Omega) Y_{l'm'}(\Omega) \beta_{lm} \beta_{l'm'} \\ &\quad - 2K_\sigma * v_i(\Omega) \sum_{l=0}^k \sum_{m=-l}^l Y_{lm}(\Omega) \beta_{lm} + K * v_i^2(\Omega). \end{aligned}$$

Since I is an unconstrained positive semidefinite quadratic program (QP) in β_{lm} , there is no unique global minimizer of I without additional linear constraints.

Integrating I further with respect to $\mu(\Omega)$, we collapse the QP to a positive definite QP, which yields a unique global minimizer as

$$\int_{S^2} I d\mu(\Omega) = \sum_{l=0}^k \sum_{m=-l}^l \beta_{lm}^2 - 2 \sum_{i=0}^k e^{-l(l+1)\sigma} \langle v_i, Y_{lm} \rangle \beta_{lm} + \sum_{i=0}^{\infty} e^{-l(l+1)\sigma} \langle v_i^2, Y_{lm} \rangle.$$

The minimum of the above integral is obtained when all the partial derivatives with respect to β_j vanish.

$$\int_{S^2} \frac{\partial I}{\partial \beta_{lm}} d\mu(\Omega) = 2\beta_{lm} - 2e^{-l(l+1)\sigma} \langle v_i, Y_{lm} \rangle = 0.$$

Hence $\sum_{l=0}^k \sum_{m=-l}^l e^{-l(l+1)\sigma} \langle v_i, Y_{lm} \rangle Y_{lm}$ is the unique minimizer in \mathcal{H}_k .

We can also show that the weighted spherical harmonic representation is related to previously available surface-based isotropic diffusion smoothing (Andrade et al. (2001), Cachia et al. (2003), Chung et al. (2003) and Chung et al. (2005)) via the following theorem.

Theorem 2.

$$\sum_{l=0}^k \sum_{m=-l}^l e^{-l(l+1)\sigma} \langle v_i, Y_{lm} \rangle Y_{lm}(\Omega) = \arg \min_{h \in \mathcal{H}_k} \|h - h_0\|,$$

where h_0 satisfies isotropic heat diffusion

$$\frac{\partial h_0}{\partial \sigma} = \Delta h_0 = \frac{1}{\sin \theta} \frac{\partial}{\partial \theta} \left(\sin \theta \frac{\partial h_0}{\partial \theta} \right) + \frac{1}{\sin^2 \theta} \frac{\partial^2 h_0}{\partial^2 \varphi}, \tag{2.9}$$

with the initial value condition $h_0(\Omega, \sigma = 0) = v_i(\Omega)$.

Proof. We first prove that heat kernel smoothing (2.7) and its spectral representation (2.8) are the solution of the heat equation (2.9). At each fixed σ , which serves as the physical time of the heat equation, the solution $h_0(\Omega, \sigma)$ belongs to $\mathcal{L}^2(S^2)$. Then the solution can be written as

$$h_0(\Omega, \sigma) = \sum_{l=0}^{\infty} \sum_{m=-l}^l c_{lm}(\sigma) Y_{lm}(\Omega). \tag{2.10}$$

Since the spherical harmonics are the eigenfunctions of the spherical Laplacian (Wahba (1990)), we have

$$\Delta Y_{lm}(\Omega) = -l(l+1)Y_{lm}(\Omega). \tag{2.11}$$

Substituting (2.10) into (2.9) and using (2.11), we obtain

$$\frac{\partial c_{lm}(\sigma)}{\partial \sigma} = -l(l+1)c_{lm}(\sigma). \tag{2.12}$$

The solution of the ordinary differential equation (2.12) is given by $c_{lm}(\sigma) = b_{lm}e^{-l(l+1)\sigma}$ for some constant b_{lm} . Hence, we obtain the solution of the form

$$h_0(\Omega, \sigma) = \sum_{l=0}^{\infty} \sum_{m=-l}^l b_{lm} e^{-l(l+1)\sigma} Y_{lm}(\Omega).$$

When $\sigma = 0$, we have the initial condition

$$h_0(\Omega, 0) = \sum_{l=0}^{\infty} \sum_{m=-l}^l b_{lm} Y_{lm}(\Omega) = v_i(\Omega).$$

The coefficients b_{lm} must be the spherical harmonic coefficients, i.e. $b_{lm} = \langle v_i, Y_{lm} \rangle$. Then from the property of the generalized Fourier series (Rudin (1991)), the finite expansion is the closest to the infinite series in \mathcal{H}_k :

$$\sum_{l=0}^k \sum_{m=-l}^l e^{-l(l+1)\sigma} \langle v_i, Y_{lm} \rangle Y_{lm}(\Omega) = \arg \min_{h \in \mathcal{H}_k} \|h - h_0(\Omega, \sigma)\|.$$

This proves the statement of the theorem.

2.3. Estimating spherical harmonic coefficients

The spherical harmonic coefficients are estimated based on an iterative procedure that utilizes the orthonormality of spherical harmonics. We assume that coordinate functions are measured at n points $\Omega_1, \dots, \Omega_n$. Then we have the normal equations

$$v_i(\Omega_j) = \sum_{l=0}^k \sum_{m=-l}^l e^{-l(l+1)\sigma} \langle v_i, Y_{lm} \rangle Y_{lm}(\Omega_j), j = 1, \dots, n. \quad (2.13)$$

The normal equations (2.13) can be written in the matrix form as

$$\mathbf{V} = \underbrace{[\mathbf{Y}_0, e^{-1(1+1)\sigma} \mathbf{Y}_1, \dots, e^{-k(k+1)\sigma} \mathbf{Y}_k]}_{\mathbf{Y}} \beta, \quad (2.14)$$

where the column vectors are $\mathbf{V} = [v_i(\Omega_1), \dots, v_i(\Omega_n)]'$ and $\beta' = (\beta'_0, \beta'_1, \dots, \beta'_k)$ with $\beta'_l = (\langle v_i, Y_{l,-l} \rangle, \dots, \langle v_i, Y_{l,l} \rangle)$. The length of the vector β is $1 + (2 \cdot 1 + 1) + \dots + (2 \cdot k + 1) = (k + 1)^2$. Each submatrix \mathbf{Y}_l is given by

$$\mathbf{Y}_l = \begin{bmatrix} Y_{l,-l}(\Omega_1), \dots, Y_{l,l}(\Omega_1) \\ \vdots & \ddots & \vdots \\ Y_{l,-l}(\Omega_n), \dots, Y_{l,l}(\Omega_n) \end{bmatrix}.$$

We may be tempted to directly estimate β in least squares fashion as $\widehat{\beta} = (\mathbf{Y}'\mathbf{Y})^{-1}\mathbf{Y}'\mathbf{V}$. However, since the size of matrix $\mathbf{Y}'\mathbf{Y}$ becomes $(k+1)^2 \times (k+1)^2$, for large degree k , it may be difficult to directly invert the matrix. Instead of directly solving the normal equations, we project the normal equations into a smaller subspace \mathcal{I}_l and estimate $2l + 1$ coefficients in an iterative fashion.

At degree 0, we write $\mathbf{V} = \mathbf{Y}_0\beta_0 + \mathbf{r}_0$, where \mathbf{r}_0 is the residual vector of estimating \mathbf{V} in subspace \mathcal{I}_0 . Note that the residual vector \mathbf{r}_0 consists of a residuals $r_0(\Omega_j)$ for all Ω_j . Then we estimate β_0 by minimizing the residual vector in least squares fashion:

$$\widehat{\beta}_0 = (\mathbf{Y}'_0\mathbf{Y}_0)^{-1}\mathbf{Y}'_0\mathbf{V} = \frac{\sum_{j=1}^n v_i(\Omega_j)Y_{00}(\Omega_j)}{\sum_{j=1}^n Y_{00}^2(\Omega_j)}.$$

At degree l , we have

$$\mathbf{r}_{l-1} = e^{-l(l+1)\sigma}\mathbf{Y}_l\beta_l + \mathbf{r}_l, \tag{2.15}$$

where the residual vector \mathbf{r}_{l-1} is obtained from the previous estimation as

$$\mathbf{r}_{l-1} = \mathbf{V} - \mathbf{Y}_0\widehat{\beta}_0 \cdots - e^{-(l-1)l\sigma}\mathbf{Y}_{l-1}\widehat{\beta}_{l-1}.$$

The least squares minimization of \mathbf{r}_l is then given by $\widehat{\beta}_l = e^{l(l+1)\sigma}(\mathbf{Y}'_l\mathbf{Y}_l)^{-1}\mathbf{Y}'_l\mathbf{r}_{l-1}$.

This iterative algorithm is referred to as the *iterative residual fitting (IRF)* algorithm (Chung et al. (2007)) since we are iteratively fitting a linear equation to the residuals obtained from the previous iteration. The IRF algorithm is similar to the *matching pursuit method* (Mallat and Zhang (1993)) although the IRF was developed independently: the IRF algorithm was developed to avoid the computational burden of inverting a huge linear problem while the matching pursuit method was originally developed to compactly decompose a time frequency signal into a linear combination of pre-selected pool of basis functions.

Although increasing the degree of the representation increases the goodness-of-fit, it also increases the number of estimated coefficients quadratically. So it is necessary to stop the iteration at the specific degree k , where the goodness-of-fit and the number of coefficients balance out. From (2.1), we can see that the k th degree weighted spherical harmonic representation can be modeled as a linear model setting:

$$v_i(\Omega_j) = \sum_{l=0}^k \sum_{m=-l}^l e^{-l(l+1)\sigma} \beta_{lm}^i Y_{lm}(\Omega_j) + \epsilon_i(\Omega_j),$$

where the least squares estimation of β_{lm}^i is $\widehat{\beta}_{lm}^i = \langle v_i, Y_{lm} \rangle$. Then we stop the iteration at degree k by testing if the $2k + 3$ coefficients at the next iteration vanish:

$$H_0 : \beta_{k+1, -(k+1)}^i = \beta_{k+1, -k}^i = \cdots = \beta_{k+1, k+1}^i = 0.$$

If we assume ϵ_i to be a Gaussian random field, the usual F test at the significant level $\alpha = 0.01$ can be used to determine the stopping degree. In our study, at bandwidth $\sigma = 0.001$, we stop the iteration at degree $k = 42$.

2.4. Validation against heat kernel smoothing

The weighted spherical harmonic representation is validated against heat kernel smoothing as formulated in Chung et al. (2005). Heat kernel smoothing was implemented as an iterated weighted averaging technique, where the weights are spatially adapted to follow the shape of heat kernel in discrete fashion along a surface mesh. The algorithm has been implemented in MATLAB and it is freely available at <http://www.stat.wisc.edu/~mchung/software/hk/hk.html>. Since its introduction in 2005, the method has been used in smoothing various cortical surface data: cortical curvatures (Luders et al. (2006) and Gaser et al. (2006)), cortical thickness (Bernal-Rusiel et al. (2008)), hippocampus (Shen et al. (2006)) magnetoencephalography (MEG) (Han et al. (2007)) and functional-MRI (Hagler Jr. (2006) and Jo et al. (2007)).

Define the n th iterated heat kernel smoothing of signal $f \in L^2(S^2)$ as

$$K_\sigma^{(n)} * f(\Omega) = \underbrace{K_\sigma * \cdots * K_\sigma}_{n \text{ times}} * f(\Omega).$$

Then we have the following theorem

Theorem 3. $K_\sigma * f(\Omega) = K_{\sigma/n}^{(n)} * f(\Omega)$.

Proof. By letting $f = Y_{l'm'}$ in (2.8), and using the orthonormality of spherical harmonics, we obtain

$$K_\sigma * Y_{l'm'}(\Omega) = \int_{S^2} K_\sigma(\Omega, \Omega') Y_{l'm'}(\Omega') d\mu(\Omega') = e^{-(l'+1)l'\sigma} Y_{l'm'}(\Omega).$$

This is the restatement of the fact that $e^{-l(l+1)\sigma}$ and $Y_{l'm'}$ are eigenvalues and eigenfunctions of the above integral equation with heat kernel. By reapplying heat kernel smoothing to (2.8), we obtain

$$K_\sigma^{(2)} * f(\Omega) = \sum_{l=0}^{\infty} \sum_{m=-l}^l e^{-l(l+1)\sigma} \langle f, Y_{lm} \rangle K_\sigma * Y_{lm}(\Omega) \quad (2.16)$$

$$= \sum_{l=0}^{\infty} \sum_{m=-l}^l e^{-l(l+1)2\sigma} \langle f, Y_{lm} \rangle Y_{lm}(\Omega). \quad (2.17)$$

Then, arguing inductively, we obtain the spectral representation of the n th iterated heat kernel smoothing as

$$K_\sigma^{(n)} * f(\Omega) = \sum_{l=0}^{\infty} \sum_{m=-l}^l e^{-l(l+1)n\sigma} \langle f, Y_{lm} \rangle Y_{lm}(\Omega).$$

The right side is the spectral representation of heat kernel smoothing with bandwidth $n\sigma$. This proves $K_\sigma^{(n)} * f(\Omega) = K_{n\sigma} * f(\Omega)$. Rescaling the bandwidth, we obtain the result.

Theorem 3 shows that heat kernel smoothing with large bandwidth σ can be decomposed into n repeated applications of heat kernel smoothing with smaller bandwidth σ/n . When the bandwidth is small, the heat kernel behaves like the Dirac-delta function and, using the *parametrix expansion* (Rosenberg (1997), Wang (1997)), we can approximate it locally using the Gaussian kernel:

$$K_\sigma(\Omega, \Omega') = \frac{1}{\sqrt{4\pi\sigma}} \exp\left[-\frac{d^2(\Omega, \Omega')}{4\sigma}\right][1 + O(\sigma^2)], \quad (2.18)$$

where $d(p, q)$ is the geodesic distance between p and q . For small bandwidth, all the kernel weights are concentrated near the center, so we need only to worry about the first neighbors of a given vertex in a surface mesh.

Let $\Omega_1, \dots, \Omega_m$ be m neighboring vertices of vertex $\Omega = \Omega_0$ in the mesh. The geodesic distance between Ω and its adjacent vertex Ω_i is the length of edge between these two vertices in the mesh. Then the discretized and normalized heat kernel is given by

$$W_\sigma(\Omega, \Omega_i) = \frac{\exp\left(-\frac{d(\Omega, \Omega_i)^2}{4\sigma}\right)}{\sum_{j=0}^m \exp\left(-\frac{d(\Omega, \Omega_j)^2}{4\sigma}\right)}.$$

Note that $\sum_{i=0}^m W_\sigma(\Omega, \Omega_i) = 1$. The discrete version of heat kernel smoothing on a triangle mesh is then defined as

$$W_\sigma * f(\Omega) = \sum_{i=0}^m W_\sigma(\Omega, \Omega_i) f(\Omega_i).$$

The discrete kernel smoothing should converge to heat kernel smoothing (2.7) as the mesh resolution increases. This is the form of the *Nadaraya-Watson estimator* (Chaudhuri and Marron (2000)) applied to surface data. Instead of performing a single kernel smoothing with large bandwidth $n\sigma$, we perform n iterated kernel smoothing with small bandwidth σ as follows $W_\sigma^{(n)} * f(\Omega)$.

For comparison between the weighted spherical harmonic representation and heat kernel smoothing, we used the sample cortical thickness data in constructing the analytical ground truth. Consider a surface measurement of the form

$$f(\Omega) = \sum_{l=0}^k \sum_{m=-l}^l \beta_{lm} Y_{lm}(\Omega) \quad (2.19)$$

for some given β_{lm} . Heat kernel smoothing of f is given as an exact analytic form, which serves as the ground truth for validation:

$$K_\sigma * f(\Omega) = \sum_{l=0}^k \sum_{m=-l}^l e^{-l(l+1)\sigma} \beta_{lm} Y_{lm}(\Omega). \quad (2.20)$$

Using the sample cortical thickness data, we simulated the measurement of the form (2.19) by estimating $\beta_{lm} = \langle f, Y_{lm} \rangle$ (Figure 3 top left). Then we compared the weighted spherical harmonic representation of f and the discrete version of heat kernel smoothing $W_{\sigma/n}^{(n)} * f$ against the analytical ground truth (2.20) (Figure 3 top right) along the surface mesh.

For the weighted spherical harmonic representation, we used $\sigma = 0.001$ and the corresponding optimal degree $k = 42$ (Figure 3 bottom left). The relative error for the weighted spherical harmonic representation is up to 0.013 at a certain vertex and the mean relative error over all mesh vertices is 0.0012. For heat kernel smoothing, we used varying numbers of iterations, $1 \leq n \leq 70$, and the corresponding bandwidth $\sigma = 0.001/n$. The performance of heat kernel smoothing depended on the number of iterations, as shown in the plot of relative error over the number of iterations in Figure 3. The minimum relative error was obtained when 21 iterations were used (Figure 3 bottom right). The relative error was up to 0.055 and the mean relative error was 0.0067. Our simulation result demonstrates that the weighted spherical harmonic representation performs better than heat kernel smoothing. The main problem with heat kernel smoothing is that the number of iterations needs to be predetermined, possibly using the proposed simulation technique. Even at the optimal iteration of 21, the weighted spherical harmonic representation provides a better performance.

2.5. Encoding surface asymmetry information

Given the weighted spherical harmonic representation, we need to establish surface correspondence between hemispheres and between subjects. This requires establishing anatomical correspondence using *surface registration*. The main motivation for the surface registration is to establish proper alignment for cortical thickness to be compared across subjects and between hemispheres. Previously, the cortical surface registration was performed by minimizing an objective function that measures the global fit of two surfaces while maximizing the smoothness of the deformation in such a way that the sulcal and gyral folding patterns are matched smoothly (Thompson and Toga (1996), Robbins (2003) and Chung et al. (2005)). In the weighted spherical harmonic representation, surface registration is straightforward and does not require any sort of explicit time consuming optimization.

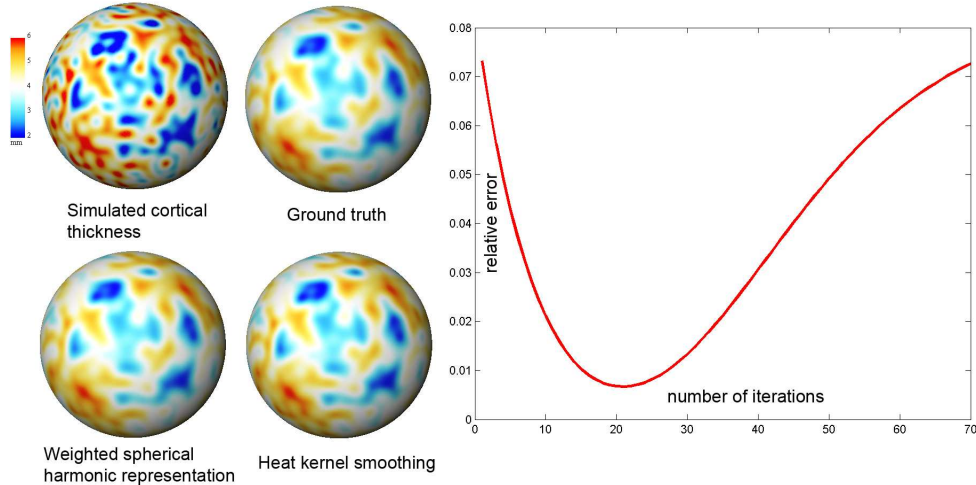


Figure 3. Cortical thickness is simulated from the sample cortical thickness. The ground truth is analytically constructed from the simulation. Then the weighted spherical harmonic representation and heat kernel smoothing of the simulated cortical thickness are compared against the ground truth. The plot is the relative error over the number of iterations for heat kernel smoothing against the ground truth.

Consider a surface \hat{h}_i obtained from coordinate functions v_i measured at points $\Omega_1, \dots, \Omega_n$:

$$\hat{h}_i(\Omega) = \sum_{l=0}^k \sum_{m=-l}^l e^{-l(l+1)\sigma} \langle v_i, Y_{lm} \rangle(\Omega).$$

Consider another surface \hat{j}_i obtained from coordinate functions w_i measured at points $\Omega'_1, \dots, \Omega'_m$:

$$\hat{j}_i(\Omega) = \sum_{l=0}^k \sum_{m=-l}^l e^{-l(l+1)\sigma} \langle w_i, Y_{lm} \rangle(\Omega).$$

Suppose the surface \hat{h}_i is deformed to $\hat{h}_i + d_i$ under the influence of the displacement vector field d_i . We wish to find d_i that minimizes the discrepancy between $\hat{h}_i + d_i$ and \hat{j}_i in the finite subspace \mathcal{H}_k . This can be easily done by noting that

$$\sum_{l=0}^k \sum_{m=-l}^l e^{-l(l+1)\sigma} (w_{lm}^i - v_{lm}^i) Y_{lm}(\Omega) = \arg \min_{d_i \in \mathcal{H}_k} \left\| \hat{h}_i + d_i - \hat{j}_i \right\|. \quad (2.21)$$

The proof of this statement is given in Chung et al. (2007). This implies that the optimal displacement in the least squares sense is obtained by simply taking the

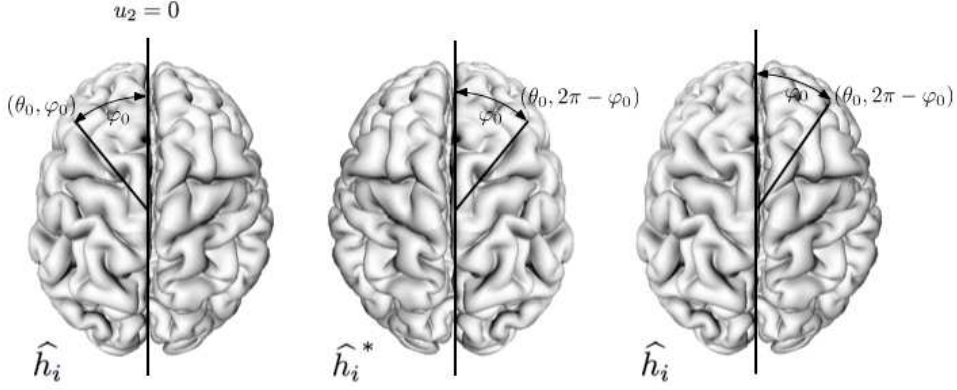


Figure 4. The point $\hat{h}_i(\theta_0, \varphi_0)$ (left) corresponds to $\hat{h}_i^*(\theta, 2\pi - \varphi_0)$ (middle) after mirror reflection with respect to the midsagittal cross section $u_2 = 0$. From the spherical harmonic correspondence, $\hat{h}_i^*(\theta, 2\pi - \varphi_0)$ corresponds to $\hat{h}_i(\theta, 2\pi - \varphi_0)$ (right). This establishes the mapping from the left hemisphere to the right hemisphere in least squares fashion.

difference between two weighted spherical harmonic representation and matching coefficients of the same degree and order. Then a specific point $\hat{h}_i(\Omega_0)$ in one surface corresponds to $\hat{j}_i(\Omega_0)$ in the other surface. We refer to this point-to-point surface correspondence as the *spherical harmonic correspondence*.

The spherical harmonic correspondence can be further used to establish the inter-hemispheric correspondence by letting \hat{j}_i be the mirror reflection of \hat{h}_i . The mirror reflection of \hat{h}_i with respect to the midsagittal cross section $u_2 = 0$ is simply given by $\hat{j}_i(\theta, \varphi) = \hat{h}_i^*(\theta, \varphi) = \hat{h}_i(\theta, 2\pi - \varphi)$, where $*$ denotes the mirror reflection operation (Figure 4). The specific point $\hat{h}_i(\theta_0, \varphi_0)$ in the left hemisphere will be mirror reflected to $\hat{j}_i(\theta_0, 2\pi - \varphi_0)$ in the right hemisphere. The spherical harmonic correspondence of $\hat{j}_i(\theta_0, 2\pi - \varphi_0)$ is $\hat{h}_i(\theta_0, 2\pi - \varphi_0)$. Hence, the point $\hat{h}_i(\theta_0, \varphi_0)$ in the left hemisphere corresponds to the point $\hat{h}_i(\theta_0, 2\pi - \varphi_0)$ in the right hemisphere. This establishes the inter-hemispheric anatomical correspondence. The schematic of obtaining this inter-hemispheric correspondence are given in Figure 4. This inter-hemispheric correspondence is used to compare cortical thickness measurements f across the hemispheres. The weighted spherical harmonic representation of cortical thickness f is

$$\hat{g}(\theta, \varphi) = \sum_{l=0}^k \sum_{m=-l}^l e^{-l(l+1)\sigma} \langle f, Y_{lm} \rangle Y_{lm}(\theta, \varphi).$$

At a given position $\hat{h}_i(\theta_0, \varphi_0)$, the corresponding cortical thickness is $\hat{g}(\theta_0, \varphi_0)$, which should be compared with the thickness $\hat{g}(\theta_0, 2\pi - \varphi_0)$ at position $\hat{h}_i(\theta_0, 2\pi -$

φ_0):

$$\widehat{g}(\theta_0, 2\pi - \varphi_0) = \sum_{l=0}^k \sum_{m=-l}^l e^{-l(l+1)\sigma} \langle f, Y_{lm} \rangle Y_{lm}(\theta, 2\pi - \varphi). \quad (2.22)$$

The equation (2.22) can be rewritten using the property of spherical harmonics:

$$Y_{lm}(\theta, 2\pi - \varphi) = \begin{cases} -Y_{lm}(\theta, \varphi), & -l \leq m \leq -1, \\ Y_{lm}(\theta, \varphi), & 0 \leq m \leq l, \end{cases}$$

$$\begin{aligned} \widehat{g}(\theta_0, 2\pi - \varphi_0) &= \sum_{l=0}^k \sum_{m=-l}^{-1} e^{-l(l+1)\sigma} \langle f, Y_{lm} \rangle Y_{lm}(\theta_0, \varphi_0) \\ &\quad - \sum_{l=0}^k \sum_{m=0}^l e^{-l(l+1)\sigma} \langle f, Y_{lm} \rangle Y_{lm}(\theta_0, \varphi_0). \end{aligned}$$

Comparing with the expansion for $\widehat{g}(\theta_0, \varphi_0)$, we see that the negative order terms are invariant while the positive order terms change sign. Hence we define the *symmetry index* as

$$S(\theta, \varphi) = \frac{1}{2} [\widehat{g}(\theta, \varphi) + \widehat{g}(\theta, 2\pi - \varphi)] = \sum_{l=0}^k \sum_{m=-l}^{-1} e^{-l(l+1)\sigma} \langle f, Y_{lm} \rangle Y_{lm}(\theta_0, \varphi_0),$$

the *asymmetry index* as

$$A(\theta, \varphi) = \frac{1}{2} [\widehat{g}(\theta, \varphi) - \widehat{g}(\theta, 2\pi - \varphi)] = \sum_{l=0}^k \sum_{m=0}^l e^{-l(l+1)\sigma} \langle f, Y_{lm} \rangle Y_{lm}(\theta_0, \varphi_0).$$

We normalize the asymmetry index by dividing it by the symmetry index as

$$N(\theta, \varphi) = \frac{\widehat{g}(\theta, \varphi) - \widehat{g}(\theta, 2\pi - \varphi)}{\widehat{g}(\theta, \varphi) + \widehat{g}(\theta, 2\pi - \varphi)} = \frac{\sum_{l=1}^k \sum_{m=-l}^{-1} e^{-l(l+1)\sigma} \langle f, Y_{lm} \rangle Y_{lm}(\theta, \varphi)}{\sum_{l=0}^k \sum_{m=0}^l e^{-l(l+1)\sigma} \langle f, Y_{lm} \rangle Y_{lm}(\theta, \varphi)}.$$

We refer to this index as the *normalized asymmetry index*. The numerator is the sum of all negative orders while the denominator is the sum of all positive and the 0th orders. Note that $N(\theta, 0) = N(\theta, \pi) = 0$. This index is intuitively interpreted as the normalized difference between cortical thickness in the left and the right hemispheres. Note that the larger the value of the index, the larger the amount of asymmetry. The index is invariant under the affine scaling of the human brain so it is not necessary to control for the global brain size difference in the later statistical analysis. Figure 5 shows the asymmetry index for three subjects.

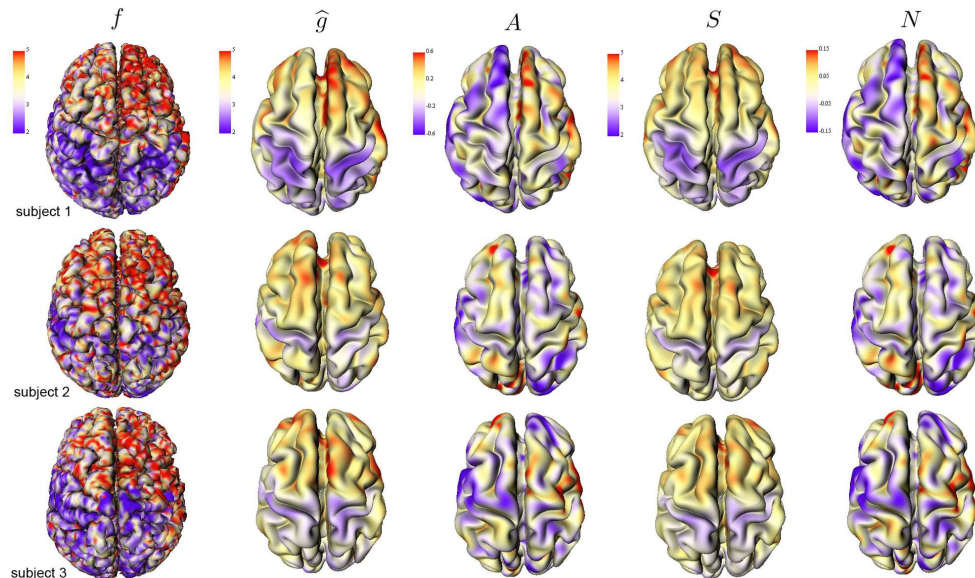


Figure 5. Three representative subjects showing cortical thickness (f), its weighted-SPHARM representation (\hat{g}), asymmetry index (A), symmetry index (S) and normalized asymmetry index (N). The Cortical thickness is projected onto the original brain surfaces while all other measurements are projected onto the 42th degree weighed spherical harmonic representation.

3. Application to Autism Study

3.1. Description of data set

Three Tesla T_1 -weighted MR scans were acquired for 16 high functioning autistic and 12 control right handed males. The autistic subjects were diagnosed by a trained and certified psychologist at the Waisman center at the University of Wisconsin-Madison (Dalton et al. (2005)). The average ages were 17.1 ± 2.8 and 16.1 ± 4.5 for control and autistic groups respectively. Image intensity nonuniformity was corrected using a nonparametric nonuniform intensity normalization method (Sled et al. (1988)), and then the image was spatially normalized into the Montreal neurological institute stereotaxic space using a global affine transformation (Collins et al. (1994)). Afterward, an automatic tissue-segmentation algorithm based on a supervised artificial neural network classifier was used to segment gray and white matters (Kollakian (1996)).

Triangle meshes for outer cortical surfaces were obtained by a deformable surface algorithm (MacDonald et al. (2000)) and the mesh vertex coordinates v_i were obtained. At each vertex, cortical thickness f was also measured. Once we obtained the outer cortical surfaces of 28 subjects, the weighted spherical

harmonic representations \widehat{h}_i were constructed. We used bandwidth $\sigma = 0.001$ corresponding to $k = 42$ degrees. The weighted spherical harmonic representations for three representative subjects are given in Figure 5. The symmetry (S), asymmetry (A) and normalized asymmetry (N) indices are computed. The normalized asymmetry index is used in localizing the regions of cortical asymmetry difference between the two groups. These indices are projected on the average cortical surface (Figure 5). The average cortical surface is constructed by averaging the Fourier coefficients of all subjects within the same spherical harmonics basis following the spherical harmonic correspondence. The average surface serves as an anatomical landmark for displaying these indices as well as for projecting the final statistical analysis results in the next section.

3.2. Statistical inference on surface asymmetry

For each subject, the normalized asymmetry index $A(\theta, \varphi)$ was computed and modeled as a Gaussian random field. The null hypothesis is that $A(\theta, \varphi)$ is identical in the both groups for all (θ, φ) , while the alternate hypothesis is that there is a specific point (θ_0, φ_0) at which the normalized asymmetry index is different. The group difference on the normalized asymmetry index was tested using the T random field, denoted as $T(\theta, \varphi)$. Since we need to perform the test on every points on the cortical surface, it becomes a multiple comparison problem. We used the random field theory-based t statistic thresholding to determine statistical significance (Worsley et al. (1996)). The probability of obtaining false positives for the one-sided alternate hypothesis is given by

$$P\left[\sup_{(\theta, \varphi) \in S^2} T(\theta, \varphi) > h\right] \approx \sum_{d=0}^2 R_d(S^2) \mu_d(h), \quad (3.1)$$

where R_d is the d -dimensional *Resel* of S^2 , and ρ_d is the d -dimensional *Euler characteristic (EC) density* of the T -field (Worsley et al. (1996) and Worsley et al. (2004)). The Resels are

$$R_0(S^2) = 2, R_1(S^2) = 0, R_2(S^2) = \frac{4\pi}{\text{FWHM}^2},$$

where FWHM is the *full width at the half maximum* of the smoothing kernel. The FWHM of the heat kernel used in the weighted spherical harmonic representation is not given in a closed form, so it is computed numerically. From (2.6), the maximum of the heat kernel is obtained when $\Omega \cdot \Omega' = 1$. Then we numerically solve for $\Omega \cdot \Omega'$:

$$\frac{1}{2} \sum_{l=0}^k \frac{2l+1}{4\pi} e^{-l(l+1)\sigma} = \sum_{l=0}^k \frac{2l+1}{4\pi} e^{-l(l+1)\sigma} P_l^0(\Omega \cdot \Omega').$$

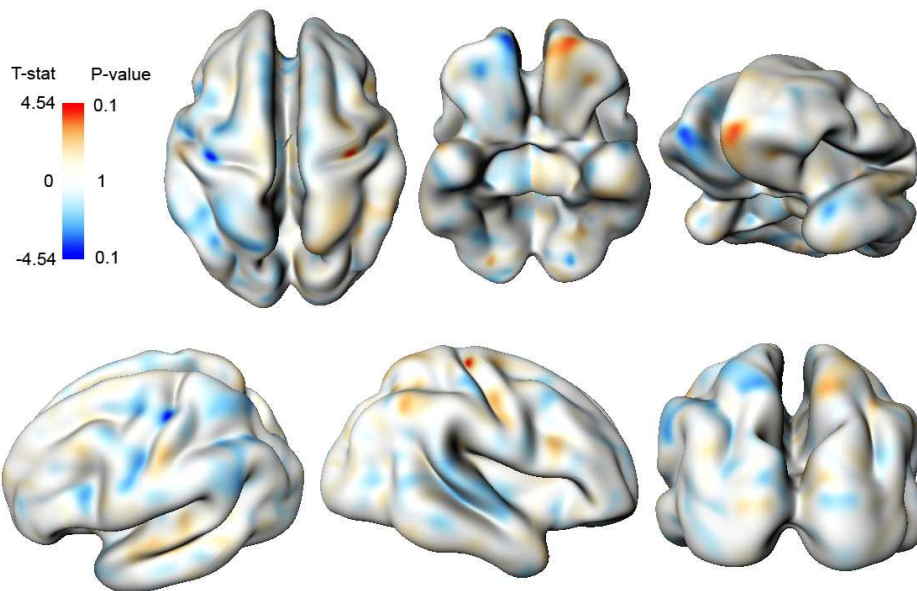


Figure 6. The statistically significant regions of cortical asymmetry thresholded at the corrected P-value of 0.1. The P-value has been corrected for multiple comparisons.

In previous surface data smoothing techniques (Chung et al. (2003) and Chung et al. (2005)), a FWHM of between 20 to 30 mm was used for smoothing data directly along the brain surface. In our study, we used a substantially smaller FWHM since the analysis is performed on the unit sphere, which has smaller surface area. The compatible Resels of the unit sphere can be obtained by using the bandwidth of $\sigma = 0.001$, which corresponds to a FWHM of 0.0968 mm. Then, based on the formula (3.1), we computed the multiple-comparison-corrected P-value and thresholded at $\alpha = 0.1$ (Figure 6). We found that the central sulci and the prefrontal cortex exhibits abnormal cortical asymmetry pattern in autistic subjects. The larger positive t statistic value indicates thicker cortical thickness with respect to the corresponding thickness at the opposite hemisphere.

4. Conclusions

We have presented a novel cortical asymmetry technique called the weighted spherical harmonic representation that unifies surface representation, parameterization, smoothing, and registration in a unified mathematical framework. The weighed spherical representation is formulated as the least squares approximation to an isotropic heat diffusion on a unit sphere in such a way that the physical time of heat diffusion controls the amount of smoothing in the weighted spherical

harmonic representation. The methodology is used in modeling cortical surface shape asymmetry. Within this framework the asymmetry index, that measures the amount of asymmetry presented in the cortical surface, was constructed as the ratio of the weighted spherical harmonic representation of negative and positive orders. The regions of statistically different asymmetry index are localized using random field theory. As an illustration, the methodology was applied quantifying the abnormal cortical asymmetry pattern of autistic subjects. The weighted spherical harmonic representation is a very general surface shape representation so it can be used for any type of surface objects that are topologically equivalent to a unit sphere.

References

- Andrade, A., Kherif, F., Mangin, J., Worsley, K., Paradis, A., Simon, O., Dehaene, S., Le Bihan, D. and Poline, J.-B. (2001). Detection of fmri activation using cortical surface mapping. *Human Brain Mapping* **12**, 79-93.
- Ashburner, J. and Friston, K. (2000). Voxel-based morphometry - the methods. *NeuroImage* **11**, 805-821.
- Barrick, T., Mackay, C., Prima, S., maes, F., Vandermeulen, D., Crow, T. and Roberts, N. (2005). Automatic analysis of cerebral asymmetry: an exploratory study of the relationship between brain torque and planum temporale asymmetry. *NeuroImage* **24**, 678-691.
- Barta, P., Miller, M. and Qiu, A. (2005). A stochastic model for studying the laminar structure of cortex from mri. *IEEE Trans. Medical Imaging* **24**, 728-742.
- Bernal-Rusiel, J., Atienza, M. and Centero, J. (2008). Detection of focal changes in human cortical thickness: Spherical wavelets versus gaussian smoothing. *NeuroImage* **41**, 1278-1292.
- Cachia, A., Mangin, J.-F., Riviere, D., Kherif, F., Boddaert, N., Andrade, A., Papadopoulos-Orfanos, D., Poline, J.-B., Bloch, I., Zilbovicius, M., Sonigo, P., Brunelle, F. and Regis, J. (2003). A primal sketch of the cortex mean curvature: a morphogenesis based approach to study the variability of the folding patterns. *IEEE Transactions on Medical Imaging* **22**, 754-765.
- Chaudhuri, P. and Marron, J. S. (2000). Scale space view of curve estimation. *The Annals of Statistics* **28**, 408-428.
- Chung, M., Dalton, K. M., L. S., Evans, A. and Davidson, R. (2007). Weighted fourier representation and its application to quantifying the amount of gray matter. *IEEE Trans. Medical Imaging* **26**, 566-581.
- Chung, M., Robbins, S., Dalton, K.M., D. R. A. A. and Evans, A. (2005). Cortical thickness analysis in autism with heat kernel smoothing. *NeuroImage* **25**, 1256-1265.
- Chung, M., Worsley, K., Robbins, S., Paus, T., Taylor, J., Giedd, J., Rapoport, J. and Evans, A. (2003). Deformation-based surface morphometry applied to gray matter deformation. *NeuroImage* **18**, 198-213.
- Collins, D., Neelin, P., Peters, T. and Evans, A. (1994). Automatic 3d intersubject registration of mr volumetric data in standardized Talairach space. *J. Comput. Assisted Tomogr.* **18**, 192-205.

- Courant, R. and Hilbert, D. (1953). *Methods of Mathematical Physics: Volume II*. Interscience, New York, english edition.
- Dalton, K., Nacewicz, B., Johnstone, T., Schaefer, H., Gernsbacher, M., Goldsmith, H., Alexander, A. and Davidson, R. (2005). Gaze fixation and the neural circuitry of face processing in autism. *Nature Neuroscience* **8**, 519-526.
- Davatzikos, C. (1997). Spatial transformation and registration of brain images using elastically deformable models. *Comput. Vis. Image Underst.* **66**, 207-222.
- Davatzikos, C. and Bryan, R. (1995). Using a deformable surface model to obtain a shape representation of the cortex. *Proceedings of the IEEE International Conference on Computer Vision* **9**, 2122-2127.
- Fischl, B., Sereno, M., Tootell, R. and Dale, A. (1999). High-resolution intersubject averaging and a coordinate system for the cortical surface. *Hum. Brain Mapping* **8**, 272-284.
- Gaser, C., Luders, E., Thompson, P., Lee, A., Dutton, R., Geaga, J., Hayashi, K., Bellugi, U., Galaburda, A., Korenberg, J., Mills, D., Toga, A. and Reiss, A. (2006). Increased local gyrification mapped in Williams syndrome. *NeuroImage* **33**, 46-54.
- Gelb, A. (1997). The resolution of the Gibbs phenomenon for spherical harmonics. *Math. Comp.* **66**, 699-717.
- Gerig, G., Styner, M., Jones, D., Weinberger, D. and Lieberman, J. (2001). Shape analysis of brain ventricles using spharm. In *MMBIA*, 171-178.
- Gu, X., Wang, Y., Chan, T., Thompson, T. and Yau, S. (2004). Genus zero surface conformal mapping and its application to brain surface mapping. *IEEE Trans. Medical Imaging* **23**, 1-10.
- Hagler Jr., D. J., S. A. S. M. (2006). Smoothing and cluster thresholding for cortical surface-based group analysis of fmri data. *NeuroImage* **33**, 1093-1103.
- Han, J., Kim, J., Chung, C. and Park, K. (2007). Evaluation of smoothing in an iterative lp-norm minimization algorithm for surface-based source localization of meg. *Physics in Medicine and Biology* **52**, 4791-4803.
- Jo, H., Lee, J.-M., Kim, J.-H., Shin, Y.-W., Kim, I.-Y., Kwon, J. and Kim, S. (2007). Spatial accuracy of fmri activation influenced by volume- and surface-based spatial smoothing techniques. *NeuroImage* **34**, 550-564.
- Kennedy, D., O'Craven, K., Ticho, B., Goldstein, A., Makris, N. and Henson, J. (1999). Structural and functional brain asymmetries in human situs inversus totalis. *Neurology* **53**, 1260-1265.
- Kollakian, K. (1996). Performance analysis of automatic techniques for tissue classification in magnetic resonance images of the human brain. Technical Report Master's thesis, Concordia University, Montreal, Quebec, Canada.
- Luders, E., Thompson, P.M., Narr, K., Toga, A., Jancke, L. and Gaser, C. (2006). A curvature-based approach to estimate local gyrification on the cortical surface. *NeuroImage* **29**, 1224-1230.
- MacDonald, J., Kabani, N., Avis, D. and Evans, A. (2000). Automated 3-D extraction of inner and outer surfaces of cerebral cortex from mri. *NeuroImage* **12**, 340-356.
- Mallat, S. and Zhang, Z. (1993). Matching pursuits with time-frequency dictionaries. *IEEE Trans. Signal Processing* **41**, 3397-3415.
- Miller, M., Banerjee, A., Christensen, G., Joshi, S., Khaneja, N., Grenander, U. and Matejic, L. (1997). Statistical methods in computational anatomy. *Statist. Meth. Medical Res.* **6**, 267-299.

- Robbins, S. (2003). Anatomical standardization of the human brain in euclidean 3-space and on the cortical 2-manifold. Technical Report PhD thesis, School of Computer Science, McGill University, Montreal, Quebec, Canada.
- Rosenberg, S. (1997). *The Laplacian on a Riemannian Manifold*. Cambridge University Press.
- Rudin, W. (1991). *Functional Analysis*. McGraw-Hill.
- Shen, L. and Chung, M. (2006). Large-scale modeling of parametric surfaces using spherical harmonics. In *Third International Symposium on 3D Data Processing, Visualization and Transmission (3DPVT)*, 294-301.
- Shen, L., Ford, J., Makedon, F. and Saykin, A. (2004). Surface-based approach for classification of 3d neuroanatomical structures. *Intelligent Data Analysis* **8**, 519-542.
- Shen, L., Saykin, A., Chung, M., Huang, H., Ford, J., Makedon, F., McHugh, T. and Rhodes, C. (2006). Morphometric analysis of genetic variation in hippocampal shape in mild cognitive impairment: Role of an il-6 promoter polymorphism. In *Life Science Society Computational Systems Bioinformatics Conference*.
- Sled, J., Zijdenbos, A. and Evans, A. (1988). A nonparametric method for automatic correction of intensity nonuniformity in mri data. *IEEE Trans. Medical Imaging* **17**, 87-97.
- Thompson, P. and Toga, A. (1996). A surface-based technique for warping 3-dimensional images of the brain. *IEEE Trans. Medical Imaging* **15**.
- Wahba, G. (1990). *Spline Models for Observational Data*. SIAM.
- Wang, F.-Y. (1997). Sharp explicit lower bounds of heat kernels. *Ann. Probab.* **24**, 1995-2006.
- Worsley, K., Marrett, S., Neelin, P., Vandal, A., Friston, K. and Evans, A. (1996). A unified statistical approach for determining significant signals in images of cerebral activation. *Human Brain Mapping* **4**, 58-73.
- Worsley, K., Taylor, J., Tomaiuolo, F. and Lerch, J. (2004). Unified univariate and multivariate random field theory. *NeuroImage* **23**, S189-195.
- Zhu, H., Ibrahim, J., Tang, N., Rowe, D., Hao, X., Bansal, R. and Peterson, B. (2007). A statistical analysis of brain morphology using wild bootstrapping. *IEEE Trans. Medical Imaging* **26**, 954-966.

Department of Biostatistics and Medical Informatics, University of Wisconsin, Madison, WI 53705, U.S.A.

E-mail: mkchung@wisc.edu

Department of Systems Engineering, Australian National University, Canberra, ACT 0200, Australia.

E-mail: Richard.Hartley@anu.edu.au

Waisman Laboratory for Brain Imaging and Behavior, University of Wisconsin, Madison, WI 53705, U.S.A.

E-mail: kmdalton@wisc.edu

Department of Psychology and Psychiatry, University of Wisconsin, Madison, WI 53705, U.S.A.

E-mail: rjdavis@wisc.edu

(Received April 2007; accepted September 2007)